Physics Letters A 382 (2018) 300–308

Contents lists available at ScienceDirect

Physics Letters A

www.elsevier.com/locate/pla

Numerical study of solitary wave stability in cubic nonlinear Dirac equations in 1D

T.I. Lakoba

Department of Mathematics and Statistics, 16 Colchester Ave., University of Vermont, Burlington, VT 05401, USA

ARTICLE INFO

Article history:
Received 7 August 2017
Received in revised form 23 November 2017
Accepted 24 November 2017
Available online 2 December 2017
Communicated by C.R. Doering

Keywords:
Nonlinear Dirac equation
Massive Gross–Neveu model
Solitary wave stability
Method of characteristics
Split-step method

ABSTRACT

Recently there has occurred a controversy between the semi-analytical prediction of linear stability of the soliton of the massive Gross–Neveu model and direct numerical observations of its instability for small values of the frequency. We revisit the problem of numerical computation of this soliton, find a mechanism behind the numerical instability observed in earlier studies, and propose methods to stably compute the soliton over long times. Thus, we confirm the semi-analytical prediction of the soliton's being linearly stable.

1. Introduction

Solitary wave solutions of the nonlinear Dirac equations have been extensively studied in the past. For brevity we will refer to those waves as Dirac solitons, even though their governing equations are not integrable by the Inverse Scattering Transform. Recently, there has occurred a controversy between theoretical and numerical studies of stability of Dirac solitons. The authors of [1] used the Evans function approach to prove that the soliton of the Dirac equations with cubic nonlinearity in (1+1) dimensions, known as the massive Gross–Neveu model [2] (or the (1+1)-dimensional Soler model [3]), is linearly stable. The massive Gross–Neveu model has the form:

$$\begin{aligned} \psi_t + \chi_x &= \ i\,(|\psi|^2 - |\chi|^2 - 1)\psi, \\ \chi_t + \psi_x &= -i\,(|\psi|^2 - |\chi|^2 - 1)\chi\,. \end{aligned} \tag{1}$$

The standing soliton solution of this model is [4]:

$$\{\psi,\ \chi\} = \{\Psi(x),\ X(x)\}\exp[-i\Omega t], \qquad \Omega \in (0,1); \tag{2a}$$

$$\Psi(x) = \frac{\sqrt{2(1-\Omega)}\,\cosh(\beta x)}{\cosh^2(\beta x) - \mu^2\,\sinh^2(\beta x)}; \quad X(x) = i\mu\,\tanh(\beta x)\,\Psi(x); \tag{2b}$$

with $\beta = \sqrt{1-\Omega^2}$ and $\mu = \sqrt{(1-\Omega)/(1+\Omega)}$. Representative members of this family for different values of Ω are shown in Fig. 1. A moving soliton is obtained from (2) by a Lorentz transformation; see, e.g., [5,6]. We omit the corresponding equations here because we focus on how stability of the soliton is affected by the frequency Ω, whereas the soliton velocity does not affect its stability due to the Lorentz invariance of model (1).

Two remarks are in order about the terminology that we will use. First, we will refer to the soliton as linearly stable whenever any initial perturbation to it does not grow exponentially in time. In [1], this was referred to as "spectral stability", i.e. the absence of eigenvalues with a positive real part (that would lead to an exponential growth) in the spectrum of the linearized operator of system (1). In other studies of Dirac solitons (see, e.g., [7], Definition 3.4), linear instability included the possibility of a growth that is slower than exponential. We opted for including only an exponential growth into our definition of linear instability since a perturbation growing slower, say as t or t^2, that starts some ten orders of magnitude below the size of the soliton (as in typical simulations of a soliton's long-term evolution) would not be able to affect the numerical solution over the times feasible in our study. On the other hand, we did not use the term "spectral stability", as in [1], because we are concerned with dynamical simulations rather than with the spectrum of an operator. Second, we will refer to the result of [1] as semi-analytical, as the Evans function, defined analytically, was computed there numerically.

E-mail address: tlakoba@uvm.edu.

https://doi.org/10.1016/j.physleta.2017.11.032
0375-9601/

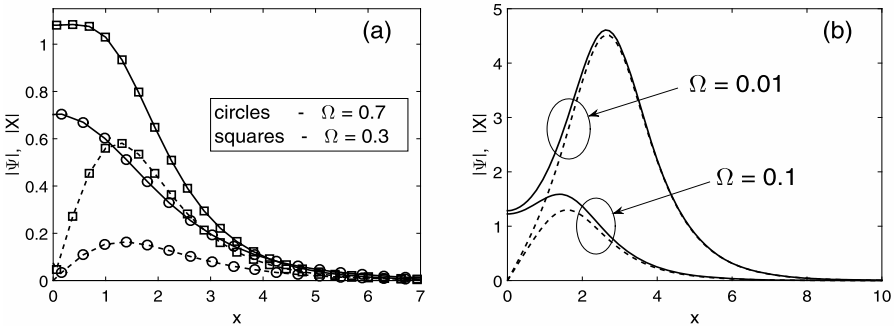

Fig. 1. Components Ψ (solid) and X (dashed) of soliton (2). By symmetry, $\Psi(-x) = \Psi(x)$ and $X(-x) = -X(x)$. Note different axes scales in panels (a) and (b), which show the soliton for intermediate (a) and small (b) values of Ω.

For our study, it is important to note that linear stability of the soliton (2) was established in [1] for all values of the frequency Ω. In [8], the eigenvalue problem obtained from model (1) linearized on the background of the soliton (2) was solved (as a particular case of a more general problem) numerically by the Chebyshev interpolation method for $\Omega = 2/3$ and $\Omega = 1/3$. Eigenvalues corresponding to a linear instability of the soliton were found in both cases. However, they were declared to be spurious, based on the fact that the respective instability growth rates decreased (albeit slowly) with the refinement of the numerical grid. Also, those — said to be spurious — growth rates were about an order of magnitude greater for $\Omega = 1/3$ than for $\Omega = 2/3$. (It should be noted that earlier [9], spurious eigenvalues in the spectrum were found, by a numerical method similar to that used in [8], for another spinor model. However, a different numerical method established [9] the absence of those spurious "unstable" eigenvalues for that other model.) In this brief overview of (semi-)analytical results for linear stability (defined above) of Gross–Neveu solitons (2) it is appropriate to mention that very recently [10], such stability was proved by purely analytical techniques, but only in the nonrelativistic limit ($\Omega \to 1$) and for nonlinearities between cubic and quintic (with the cubic one excluded) in system (1). Thus, there is still no analytical proof of linear stability of the massive Gross–Neveu soliton (2). Nonetheless, the conclusion from the semi-analytical study [1], supported by results of [8] (see also the above comment regarding [9]), is that this soliton is linearly stable for all values of its frequency Ω.

However, this conclusion was recently questioned in a systematic numerical study [11]. That study, in its turn, was motivated by a discrepancy between, on one hand, the theoretical result of [1] and an early numerical study [12], which claimed stability of the soliton (2), and, on the other hand, another early numerical study [13], which reported instability of the soliton for $\Omega = 0.5$. It should be noted that the simulation times in [12] were rather small, $t < 300$, which would not allow one to definitively state whether the soliton was stable or weakly unstable. Moreover, an unstable dynamics of solitons with $\Omega = 0.3$ was also noted in [14], although there the Dirac equations contained an external potential. Thus, the numerical evidence that had existed prior to study [11] suggested that the soliton (2) could actually be (possibly weakly) unstable for sufficiently small Ω, in contradiction to the semi-analytical result of [1].

The authors of [11] presented results of their detailed and systematic numerical simulations for Ω as low as 0.1. They reported a weak instability, which developed for $\Omega < 0.56$ over times on the order of a hundred (for $\Omega = 0.1$) or ten thousand (for $\Omega = 0.5$) time units and which could be mitigated by increasing the length of the computational domain. In [15] the numerical study of stability of soliton (2) was continued by three numerical methods different from that used in [11]. With their best-performing method and for the largest computational domain, the authors of [15] were able to defer the appearance (see the clarification below) of the instability of the soliton with $\Omega = 0.1$ to $t \sim 3000$. For $\Omega = 0.3$ and 0.5 the instability took respectively longer times to develop. (It should be clarified that Refs. [11] and [15] defined the time of appearance of an instability as that when the L_2-norm of the error in the charge density

$$\rho(x,t) \equiv |\phi|^2 + |\chi|^2 \tag{3}$$

would reach 10^{-3}.) The authors of [15] concluded that in the limit of very large domain length and very fine discretization in space and time, — even though these authors could not reach that limit — the soliton (2) is expected to be stable for all Ω, as predicted by [1]. Consequently, they pointed out that it would be important to design a numerical method that would be free of the weak instability observed for soliton (2), as well as to understand a reason for that instability, produced by various numerical methods.

In this Letter we report progress in both of these directions. First, we found the main "culprit" for the (weak) instability of the soliton with sufficiently small Ω, observed in simulations. Second, we present two simple and well-known numerical methods which are able (after one modification) to simulate soliton (2) with values of Ω of an order of magnitude smaller than reported in [11] and [15], for significantly longer times, and with significantly smaller error.

We will now discuss the "culprits" behind the numerically observed instability in [15] and [11]. In [15], this culprit is the dispersive waves "radiated" by the soliton due to discretization error. This radiation initially moves away from the soliton, but later re-enters the computational domain due to either periodic or (partially) reflecting boundary conditions (BC), such as the homogeneous Dirichlet BC. Let us note that all methods used in [15] employed one of these two types of BC. Over long times, the radiation proceeds to repeatedly propagate through the soliton and hence interacts with it. This weak interaction is what causes destruction of the soliton for sufficiently small Ω. In Section 2 we will demonstrate that when one prevents the radiation from affecting the soliton, the soliton remains stable, meaning that sufficiently small perturbation of its profile would not grow exponentially.

A culprit behind the instability observed in [11] was not the re-entering radiation. We will explain here why this is so, but will only comment briefly on the potential candidate for such a culprit in an Appendix, as this is not directly related to our own results. The numerical method employed in [11] used so-called nonreflecting BC. This name refers to the fact that most of the field that reaches the boundary is allowed (by these BC) to leak out of the computational domain, so that only a small part of it will be reflected back into the domain (see Section 2.2 below). Having such nonreflecting boundaries is desirable in simulations of solitary waves, as a large percentage of the radiation leaving the

vicinity of the wave would exit the domain and thus would not be able to affect the solitary wave. As we will show in Section 2.2, the small part of the radiation that is reflected back into the domain would not be "harmful" to the soliton for not too small Ω for times as short as those reported in [11] (see Fig. 9 there). Thus, interaction with dispersive waves would not explain most of the unstable simulations reported in [11]. We will present a hypothesis that might explain those instabilities in Appendix A. Such instabilities were not observed in our simulations, and hence their detailed analysis is outside the scope of this work.

In Section 2 below we will present two numerical methods that allowed us to simulate soliton (2) with small Ω over times much greater than $t = 1000$. These methods are: a method of characteristics (MoC) and a version of the split-step method where the linear evolution is performed by the MoC. In their original form, they are capable of simulating the soliton with the smallest value of the frequency ($\Omega = 0.1$) as, and over longer times than, reported in [11] and [15]. However, the error in the numerical solution is seen to grow, and hence a definite conclusion about the soliton's stability still cannot be made. We then show how absorbing BC can be used to eliminate that error. The results obtained with the absorbing boundaries show no sign of instability, and thereby confirm linear stability, of the soliton with $\Omega \geq 0.01$ in agreement with the semi-analytical result of [1]. In Section 3 we will summarize this work. In Appendix A we will argue that the instability observed in [11] could be a high-wavenumber instability of the numerical method rather than the property of the soliton itself. In Appendix B we will present a numerical evidence that the Fourier split-step method (as opposed to its version considered in Section 2) may be unconditionally unstable when applied to solitons (2) with sufficiently small Ω. This will justify our not using the Fourier version of the split-step method for the Gross–Neveu soliton.

2. Numerical methods and results

In Section 2.1 we will briefly review numerical methods that were previously used for the Dirac equations. Then in Section 2.2 we will present a MoC-based scheme for Eqs. (1). While it uses nonreflecting BC, we will demonstrate that part of the field gets reflected back into the computational domain. This phenomenon numerically destabilizes solitons (2) with sufficiently small Ω. Consequently, in Section 2.3, we will present and justify our choice of absorbing BC and demonstrate that they will allow to simulate the soliton with $\Omega = 0.01$ (ten times smaller than in [15]) up to $t = 10{,}000$ (over three times greater than in [15]) with an error smaller than in [15]. Finally, in Section 2.4, we will present similar results for a MoC-based version of the split-step method.

2.1. Review of earlier numerical studies of Eqs. (1)

Dynamics of solitons of the Gross–Neveu model has been extensively studied by various numerical methods: see, e.g., recent reviews [16,17] of those methods and Refs. [6,18]. Without trying to provide a comprehensive discussion of the subject, we will briefly comment on these methods while focusing on their suitability for, and results related to, our main purpose, which is simulation of solitons (2) with small Ω over *long times*.

The majority of those methods used finite differences to discretize the spatial derivatives in (1). With few exceptions [19], such methods lead to so-called "fermion doubling" and therefore are not suitable for long-time and high-accuracy simulations of Eqs. (1). "Fermion doubling" is caused by the numerical dispersion, which at high wave numbers k leads to the corresponding harmonics propagating with a group velocity that is opposite in sign to the group velocity of the physical, low-k harmonics. A problem occurs because the physical dispersion relation of the Dirac model (1) has two branches of opposite signs:

$$\omega_{\pm}(k) = \pm\sqrt{k^2 + 1}. \tag{4}$$

Therefore, the high-k (i.e., purely numerical) harmonics of one branch have the same group velocity as low-k (i.e., physical) harmonics of the other branch. Due to this group-velocity synchronism, these two groups of harmonics would then interact with each other, which can lead to numerical instability. The finite difference staggered-grid scheme proposed in [19] for the *linear* Dirac equations reproduces the exact dispersion relations (4). However, it uses the leap-frog solver, which is known to suffer from a nonlinear numerical instability (see, e.g., [21,22]), unless a certain filtering is implemented [23]. For this reason, we did not use that scheme.

Other numerical methods for model (1) include the Fourier split-step method (SSM) of second [24,17] and fourth order [16], exponential time-differencing (also called "exponential wave") Fourier methods [6,17], and a wavelet-based method [18]. It should be noted that both Fourier methods — SSM and exponential time-differencing — preserve the exact dispersion relation (4). However, their drawback is that they employ periodic BC, which allows dispersive radiation to repeatedly re-enter the computational domain and thereby, as we have pointed out earlier, to destabilize the soliton. To prevent this from occurring, artificial numerical absorption is to be introduced at the boundaries. We have observed that while the so modified Fourier SSM can stably simulate the Gross–Neveu soliton with smaller values of the frequency than which was previously achieved in [11] and [15], its performance is significantly inferior to that of the two methods whose results we will present in this work. In Appendix B we will also report on instances of *unconditional* numerical instability of the Fourier SSM, which contradicts the method's stability property claimed in [24,16]. For these reasons, we did not use the Fourier SSM in this work.

It should be noted that, to our knowledge, most studies of the dynamics of soliton (2) were obtained for times that were less or on the order of 100 time units. Two exceptions (in addition to Refs. [11] and [15], which have been reviewed in detail above) are Refs. [5,25], which studied collisions of two and three solitons, reporting some of their longer simulations up to $t = 500$. In the subset of those studies which reported simulations of solitons with $\Omega < 0.7$, higher sensitivity to perturbations of solitons with smaller values of the frequency was evident even for $t \sim 100$. The methods that we will propose below are able to stably simulate solitons (2) with significantly smaller values of the frequency (and hence more sensitive to perturbations) than what was done before, and over significantly longer times.

2.2. Method of characteristics (MoC) with nonreflecting BC for Eqs. (1)

By a change of variables

$$u = (\psi + \chi)/\sqrt{2}, \qquad v = (\psi - \chi)/\sqrt{2}, \tag{5}$$

Eqs. (1) take on the form:

$$\begin{aligned} u_t + u_x &= i(|v|^2 u + v^2 u^*) - iv \equiv f_{(u)}(u, v), \\ v_t - v_x &= i(|u|^2 v + u^2 v^*) - iu \equiv f_{(v)}(u, v). \end{aligned} \tag{6}$$

Since the computational domain $x \in [-L/2,\ L/2]$ is typically taken to be so large that the field at its boundaries is smaller than the machine round-off error, it is appropriate to impose the nonreflecting BC, mentioned in the Introduction:

$$u(-L/2, t) = 0, \qquad v(L/2, t) = 0. \tag{7}$$

In characteristic coordinates

$$\xi = (t-x)/2, \qquad \eta = (t+x)/2, \tag{8a}$$

Eqs. (6) are rewritten as:

$$\begin{aligned} u_\eta &= i(|v|^2 u + v^2 u^*) - iv, \\ v_\xi &= i(|u|^2 v + u^2 v^*) - iu. \end{aligned} \tag{8b}$$

The idea of the MoC is that each of the equations in (8) is solved as an ordinary differential equation (ODE) with respect to the corresponding characteristic coordinate. Thus, the numerical MoC has different "flavors" depending on which ODE numerical solver is used. In [26] we showed that for a class of energy-preserving systems, to which the Dirac model belongs, the modified Euler (ME) solver *with the nonreflecting BC* (7) renders the corresponding MoC flavor *almost* (see below) stable, provided that

$$h\, e^{\text{const}\cdot Lh} < 1, \tag{9}$$

where h is the discretization step in time and space (see text after (11)). The constant in the exponent in (9) has magnitude $O(1)$ and depends on the right-hand side of (8b). Its general expression was not derived in [26], but in each particular case the length L of the computational domain can be adjusted by a quick trial and error to satisfy the stability condition (9). The word "almost" three sentences above means that a mild instability occurs only for a small number of lowest- and highest-wavenumber harmonics and has the growth rate

$$\gamma_{\text{ME}} = O(h^3). \tag{10}$$

That is, the aforementioned modes grow as $\exp[\gamma_{\text{ME}} t]$, while modes in other parts of the spectrum remain stable, provided that (9) holds. This mild instability is well-known for the ME method applied to energy-preserving ODEs (see, e.g., [27]). By a proper choice of h it can be made weak enough so as not to affect the numerical solution over a given time.

The numerical scheme of the MoC with the ME solver (to be referred to as the MoC-ME) is:

$$\begin{aligned} \overline{u}_m &= u^n_{m-1} + h\, f_{(u)}\left(u^n_{m-1},\, v^n_{m-1}\right), \\ \overline{v}_m &= v^n_{m+1} + h\, f_{(v)}\left(u^n_{m+1},\, v^n_{m+1}\right); \end{aligned} \tag{11a}$$

$$\begin{aligned} u^{n+1}_m &= \frac{1}{2}\left[\, u^n_{m-1} + \overline{u}_m + h\, f_{(u)}\left(\overline{u}_m,\, \overline{v}_m\right)\right], \\ v^{n+1}_m &= \frac{1}{2}\left[\, v^n_{m+1} + \overline{v}_m + h\, f_{(v)}\left(\overline{u}_m,\, \overline{v}_m\right)\right]; \end{aligned} \tag{11b}$$

Here $\{u, v\}^n_m \equiv \{u, v\}(x_m, t_n)$ and $f_{\{(u),(v)\}}$ are the functions on the right-hand side of Eqs. (6). The discretization steps in time and space are taken to be equal: $\Delta t = \Delta x = h$, so that the integration in (11) proceeds along the characteristic directions (8a). Namely, the first (second) equation in (11a) "predicts", by the simple Euler method, the new value of u (v) along the characteristic $\xi = \text{const}$ ($\eta = \text{const}$), which connects node (x_{m-1}, t_n) (node (x_{m+1}, t_n)) to node (x_m, t_{n+1}). Then the first (second) equation in (11b) "corrects", by the trapezoidal rule, the value of u (v) at node (x_m, t_{n+1}). Thus, the MoC-ME inherits the $O(h^2)$ accuracy from its counterpart for ODEs.

The BC for scheme (11) follow from (7):

$$u^n_1 = 0, \qquad v^n_M = 0, \qquad n \geq 0, \tag{12}$$

where M is the number of grid points in space. As we noted in the Introduction, these BC allow most of the field that has propagated from inside the computational domain to its boundaries to leak out and not be reflected back into the domain. This is a desirable property for simulations of solitary waves. However, BC (7) are truly nonreflecting only when $f_{\{(u),(v)\}} \equiv 0$ and are almost nonreflecting for high-frequency harmonics, when each term on the left-hand side of (6) dominates the respective right-hand-side terms. In Fig. 2 we illustrate that in the general case, while these BC let some of the field leak out of the computational domain, such a leakage occurs rather slowly after the instance when the field first reaches the boundary of the domain (which in Fig. 2 is for $t \approx L/2 = 32$). It should be noted that the higher the frequency of the modes, the higher the rate of their leakage out of the computational domain.

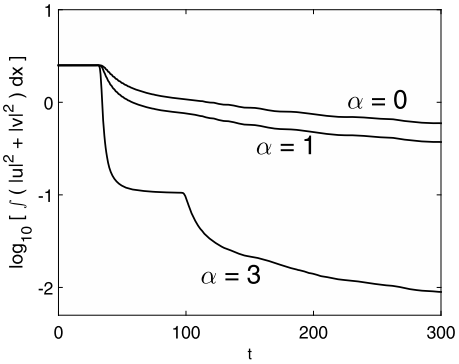

Fig. 2. Evolution of the L_2-norm of the solution of a linear counterpart of system (6) with $f_{(u)} = -iv$, $f_{(v)} = -iu$ with nonreflecting BC (7) and the initial condition $u(x,0) = v(x,0) = \exp[-x^2 - i\alpha x]$, where values of α are marked in the plot. Note that higher values of α correspond to a greater share of high-frequency harmonics in the initial condition. Length of computational domain is $L = 64$.

Even this incomplete leakage of dispersive radiation out of the computational domain suffices to prevent it from destroying the Gross–Neveu soliton (2) with a "not too small" Ω over "not too large" times. Fig. 3(a) shows the numerical solution for $\Omega = 0.1$ (the smallest value of the frequency reported in [11,15]) obtained by the MoC-ME (11) with nonreflecting BC (12) at $t = 1{,}000$ and $t = 4{,}000$. Note that the time $t = 4{,}000$ is about 30% greater than that reported in [15] for approximately the same error.

The amount of radiation emitted by the soliton, as seen in Fig. 3(a), may be used as an indicator of the soliton's numerical stability. With this indicator, our simulations confirmed the observations of earlier numerical studies that the soliton becomes increasingly more (less) susceptible to the effect of a small but finite discretization error of the numerical scheme as one decreases (increases) Ω. For example, for the same simulation parameters as in Fig. 3 but for the soliton with $\Omega = 0.07$, the radiation reaches the level of 10^{-4} already by $t = 1{,}000$. On the other hand, the radiation from a soliton with $\Omega = 0.15$ remains below 10^{-4} even for $t = 10{,}000$. In Fig. 3(b) we also show the time evolution of the L_2-norm of the radiation, which for the purpose of this illustration we defined as

$$Q_{\text{radiation}} = \left(\int_{-L/2}^{-L/4} + \int_{L/4}^{L/2}\right)(|u|^2 + |v|^2)\, dx, \tag{13}$$

for three decreasing values of Ω. The increased rate, as Ω decreases, at which the soliton emits radiation and hence disintegrates, is evident from Fig. 3(b). Conversely, the robustness of the soliton to the destabilizing effect of the radiation rapidly increases with increasing Ω. For example, the radiation of solitons with $\Omega = 0.2$ and $\Omega = 0.3$ remains below 10^{-7} at $t = 10{,}000$, with other numerical parameters being the same as in Fig. 3. Thus, below we will quote the results only for the soliton with the smallest Ω that we have simulated; the corresponding results for solitons

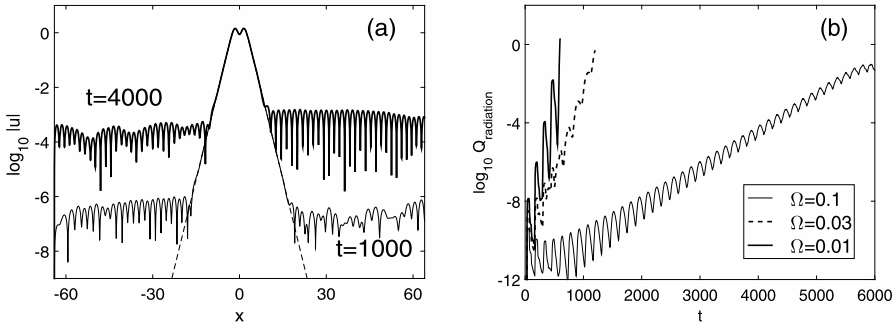

Fig. 3. Panel (a): Solution of (6) with the MoC-ME (11) and nonreflecting BC (12) at $t = 1000$ (thin line) and $t = 4000$ (thicker line). The initial condition is soliton (2) (see also (5)) with $\Omega = 0.1$, depicted with the dashed line. (In linear scale this soliton is shown in Fig. 1(b).) Component $|v|$ appears as a replica of $|u|$ reflected about $x = 0$. Simulation parameters: $L = 128$, $M = 3 \cdot 2^{13} \approx 25{,}000$, $h \approx 0.005$. Panel (b): Time evolution of the field's L_2-norm outside of the soliton, as defined in (13). The simulation parameters are the same as in panel (a), except that the initial conditions are the solitons with the values of Ω listed in the legend.

with higher Ω do not need to be presented as they are guaranteed to be better.

At the same time, the radiation emitted by the soliton may also be *an agent* that destabilizes the soliton. Indeed, originally, the radiation is produced by the soliton due to the discretization error of the numerical scheme However, a significantly greater amount of radiation appears to be produced at later stages of the evolution when part of the "original" radiation re-enters the computational domain and subsequently interacts with the soliton, causing it to radiate more. It is either this mechanism, or else a true linear instability of the soliton, that can explain a several hundred-fold increase of the amount of radiation, seen in Fig. 3(a), when the simulation time increases by a mere factor of four, from $t = 1{,}000$ to $t = 4{,}000$. To establish which of the two mechanisms takes place, and thus whether a small-Ω soliton is linearly stable, we need to eliminate the possibility for the radiation to re-enter the computational domain and see whether this would "stabilize" the numerically computed soliton. To that end we employed absorbing BC, whose choice is justified in the next subsection.

2.3. Absorbing BC, and simulations of a small-Ω soliton with the MoC-ME

We will begin by briefly reviewing three established techniques of imposing absorbing BC. Given their known drawbacks or similar issues, we will then present another, much simpler, technique and will demonstrate its effectiveness in "stabilizing" the numerically computed soliton with small Ω over long times.

One technique consists of explicitly requiring that all numerically resolved modes propagating, say, to the left become zero at the left boundary (and similarly for the right boundary). Imposition of this requirement results into so-called Dirichlet-to-Neumann or Neumann-to-Dirichlet maps, which amount to solving an integro-differential equation in time which is also nonlocal in space. Explicit examples of using this technique can be found, e.g., in [20] for the simple, first-order wave equation and in [19] for the staggered-grid leap-frog scheme for the linear Dirac equations; more references can be found in a review [28]. An obvious issue with this technique is that the solution of the aforementioned integro-differential equation at each time step increases the computational cost of the numerical scheme (not to mention that it makes it conceptually more complex). Another issue is that the discretization of this integro-differential equation must be performed consistently with the finite-difference scheme for the evolution equations themselves; otherwise a weak numerical instability may arise [20,19]. Ensuring this consistent discretization adds to the complexity of the scheme.

Another technique consists of introducing a so-called perfectly matched layer (PML) around the "useful" part of the computational domain. The role of the PML is to absorb the radiation which has entered the PML and not to have any part of that radiation to be reflected back into the "useful" computational domain. To that end, both the width of the PML and the "absorbing function" must be chosen carefully [28], by experimentation. While this is not a drawback, it does make the PML technique semi-empirical.

The third technique is to apply so-called (high-order) local nonreflecting BC; see, e.g., [29] and a review [30]. This technique completely suppresses the re-entering of a small number of modes of the radiation while strongly suppressing the re-entering of most other modes. It requires the solution of a set of time-dependent ODEs at the boundaries, with certain parameters of this set being selected, in part, empirically (although general guidelines for that exist).

The common feature of all of these three techniques is that they require additional coding to ensure the desired properties at the boundaries. At least for the first technique, this additional coding is quite substantial. In the other two techniques, while the additional coding may be less complex, one requires an "educated guess" of certain parameters.

As a simple alternative to these techniques, we multiplied the solution at every time step[1] by an "absorber" function:

$$a(x) = \begin{cases} 1, & |x| < L_1; \\ \exp\big[-\big((|x| - L_1)/W\big)^2\big], & |x| \in [L_1,\, L/2]; \end{cases}$$
$$W = (L/2 - L_1)/B\,. \tag{14a}$$

As the latter two of the above techniques, this requires some guesswork of the absorber's parameters L_1 and B. The nonabsorbing part, $[-L_1, L_1]$, of the computational domain can be selected from the observation that the solution should not be modified only where the exact solution exceeds the discretization error. Using the $t = 1000$ data from Fig. 3(a), one concludes that one can take $L_1 \gtrsim 0.3 \cdot (L/2)$.

To select a value for B, note that it relates to the absorber's value at the boundary as follows:

$$a(\pm L/2) = \exp\big[-B^2\big]. \tag{14b}$$

Using a greater B does *not* necessarily result in stronger absorption because multiplication of the solution by an absorber gives rise to the introduction into the evolution equation of an effective "potential", which usually leads to reflection of part of the radiation. The smaller B, the weaker this reflection. Thus, a balance between having, on one hand, sufficient absorption at the boundaries and, on

[1] This could be changed, of course, resulting in a less aggressive imposition of absorbing BC.

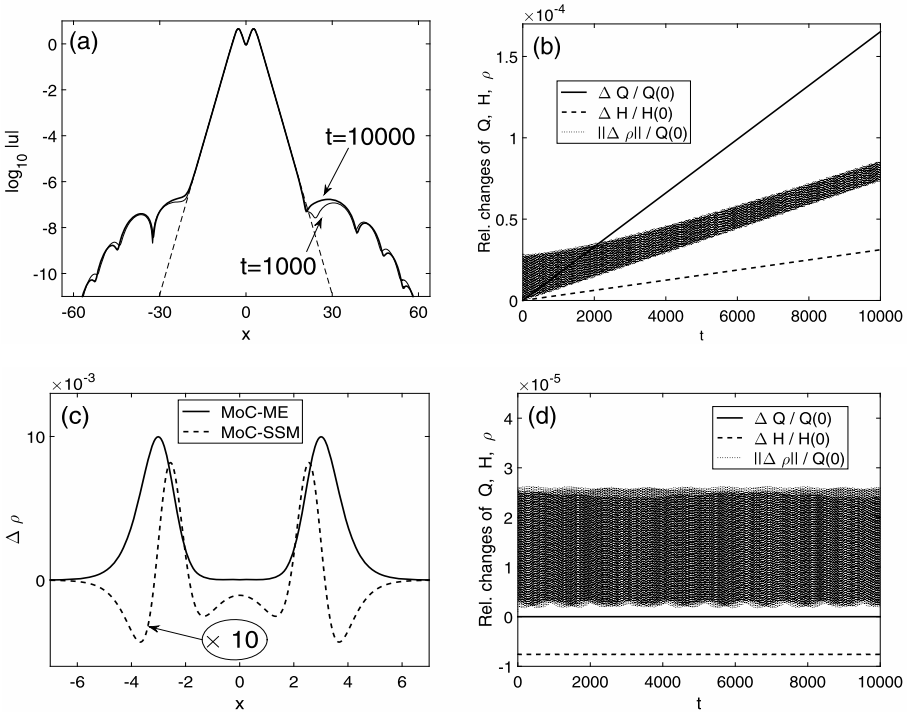

Fig. 4. Solution of (6) with the MoC-ME (11) (panels (a), (b), and (c)) or MoC-SSM (19b) (panels (c) and (d)), nonreflecting BC (12), and an additional absorbing boundaries imposed by (14a), (15) at every time step. Panel (a): The initial condition (dashed line) is soliton (2) (see also (5)) with $\Omega = 0.01$; thin line – at $t = 1000$; thicker line – at $t = 10{,}000$. In linear scale the initial soliton is shown in Fig. 1(b). Other simulation parameters are the same as in Fig. 3. The numerical solution obtained with the MoC-based SSM looks similar and therefore is not shown. Panel (b): Relative deviation of conserved quantities (16b) and the L_2-norm of the deviation of the charge density (17) for the solution obtained with the MoC-ME. A band, instead of a curve, appears for the $\|\Delta\rho\|$ because that quantity oscillates with a period of order $O(1)$. Panel (c): Spatial profiles of $\Delta\rho$ at $t = 10{,}000$. The profile obtained by the MoC-SSM had to be magnified by the factor 10 to be clearly visible on the same scale as the other curve. Panel (d): Same quantities as in (b), but for the solution obtained by the MoC-SSM. Note that the charge stayed exactly constant, which is a well-known property of the SSM (see, e.g., [24]).

the other hand, small enough reflection inside the absorber, is to be achieved by properly selecting a value of B. There are no specific guidelines for choosing that value, but it can usually be found in each particular case by a quick experimentation. Thus, using the above observation for L_1 and a trial and error for B, in the simulations reported below we used

$$L_1 = 0.4 \cdot (L/2), \qquad B = 0.05. \tag{15}$$

These values may not be optimal, but they were sufficient for our purpose.

Fig. 4(a) shows the result of simulating a soliton with $\Omega = 0.01$ (ten times smaller than in [15]) by the MoC-ME (11) with nonreflecting BC (12) and additional absorbing boundaries imposed by (14a), (15) at every time step. One can see that the amount of radiation remains practically unchanged from $t = 1{,}000$ to $t = 10{,}000$ and stays below the 10^{-6} level. This proves that the soliton is linearly stable, and the instability of low-Ω solitons observed in previous numerical studies was due to the interaction of dispersive waves with the soliton.

In Fig. 4(b) we show the evolution of numerically computed quantities $Q(t)$ (charge) and $H(t)$ (Hamiltonian) that are conserved in the exact Gross–Neveu model (1). In the original variables, they are:

$$\begin{aligned} Q &= \int \left(|\psi|^2 + |\chi|^2\right) dx; \\ H &= \int \Big[-i(\psi^*\chi_x + \chi^*\psi_x) - \frac{1}{2}(|\psi|^2 - |\chi|^2)^2 \\ &\quad + (|\psi|^2 - |\chi|^2) \Big] dx; \end{aligned} \tag{16a}$$

in the characteristic variables (5) they are:

$$\begin{aligned} Q &= \int \left(|u|^2 + |v|^2\right) dx; \\ H &= \int \Big[-i(u^*u_x - v^*v_x) - \frac{1}{2}(uv^* + u^*v)^2 \\ &\quad + (uv^* + u^*v) \Big] dx. \end{aligned} \tag{16b}$$

We also plot the L_2-norm of the deviation of the charge density, defined by

$$\Delta\rho(x,t) = \rho(x,t) - \rho(x,0), \tag{17}$$

where $\rho(x,t)$ was defined in (3). This deviation was used as the measure of error in [11,15]. A typical spatial profile of this deviation is shown in Fig. 4(c).

The observed growth of Q, H, and $\|\Delta\rho\|$ is due to the mild, low-wavenumber instability of the MoC-ME, "inherited" from the ME method for ODEs. According to (10), this growth rate of the deviations of Q and H from their initial values should scale as h^3. We confirmed this by repeating the simulations with parameters of Fig. 4 except for doubling M to $3 \cdot 2^{14}$, resulting in halving h. The corresponding relative deviations of Q and H, multiplied by 8 ($= 2^3$), are almost indistinguishable from their respective counterparts in Fig. 4(b). The initial (at $t = 1$) value of $\|\Delta\rho\|$ was found to be 4 ($= 2^2$) times smaller than that in Fig. 4(b); this is because this deviation is initially created by the discretization error of the *2nd-order accurate* MoC-ME. However, its growth rate over long times was found to be 8 ($= 2^3$) times smaller than for $M = 3 \cdot 2^{13}$, in agreement with the growth rate of the low-k harmonics given by (10).

The method that we will present in the next subsection is free from this systematic growth of the above quantities.

Let us also remind the reader that, as we pointed out at the end of Section 2.2, solitons with $\Omega > 0.01$ are even more robust than that with $\Omega = 0.01$. For example, for $\Omega = 0.1$ and 0.2 and for

other simulation parameters being the same as in Fig. 4, the radiation outside of the soliton is below 10^{-11} and 10^{-12}, respectively, i.e., more than four (respectively, five) orders of magnitude smaller than in Fig. 4(a).

2.4. Split-step method with MoC-based linear substep

The SSM, proposed for evolution equations in the 1960s, was first applied to nonlinear Dirac equations in [24]. The idea of the method is that the a time step is split into two types of substeps. In one type of substeps, one solves the evolution occurring only due to the x-derivative terms in (1), while in the other type of substeps one exactly solves nonlinear *ODEs* corresponding to the remaining terms. By alternating these substeps with specially selected weights, one can construct SSMs of arbitrarily high orders in Δt (see, e.g., [31]).

The most common method to execute the substep with linear x-derivative terms is to use discrete Fourier transform (DFT). It is this version of the SSM that was proposed in [24] and later used in [16,17]. However, by virtue of its using the DFT, this version of the SSM imposes periodic BC. Such BC let the radiation re-enter the computational domain, which, as we have seen in previous subsections, leads to destabilization of solitons with sufficiently small Ω; therefore, the Fourier SSM is unsuitable for our purpose of long-time stability study of solitons. Moreover, as we demonstrate in Appendix B, the Fourier SSM may become *unconditionally* (i.e., for an arbitrarily small Δt) unstable, in contradiction to what was stated in [24,17].

Fortunately, it is easy to execute the substep which accounts for the linear x-derivative terms (1) by a different method. Namely, the change of variables (5) and (8a) shows that at this substep, $u^{(\mathrm{lin})}(x,t) = u^{(\mathrm{lin})}(x-t)$ and $v^{(\mathrm{lin})}(x,t) = v^{(\mathrm{lin})}(x+t)$. On a grid, this can be implemented as

$$(u^{(\mathrm{lin})})_m^{n+1} = (u^{(\mathrm{lin})})_{m-1}^n, \qquad (v^{(\mathrm{lin})})_m^{n+1} = (v^{(\mathrm{lin})})_{m+1}^n, \tag{18}$$

where the notations were introduced after (11). To complete the numerical implementation of this substep, one inverts transformation (5) to obtain $\psi^{(\mathrm{lin})}$ and $\chi^{(\mathrm{lin})}$ at the $(n+1)$th time level. Given an obvious relation of the implementation of this substep with the MoC, we will refer to this version of the SSM as the MoC-SSM.

Let us note that the MoC-SSM is about twice as fast as the Fourier SSM because instead of using direct and inverse DFT, one needs to perform only the much simpler transformation (5) and its inverse and to re-assign values of the intermediate solution according to (18). *Much more importantly*, however, the MoC-SSM can use the nonreflecting BC (12). This makes it less plagued by the problem of the re-entering radiation, just as this was the case for the MoC-ME in Section 2.2.

The MoC-SSM was mentioned in [16] and employed in the stability study of soliton (2) in [11]. Surprisingly in view of what we said in the previous paragraph, its performance was found to be inferior to the Fourier collocation method used in [15]. Moreover, the presence of numerically unstable highly-oscillatory modes can be discerned from Figs. 5 and 6 and their captions in [11]. In Appendix A we will argue that this could be the consequence of using a 4th-order accurate form of the SSM. Therefore, below we will report results only for the 2nd-order accurate form [32] of the MoC-SSM. Namely, if one writes Eqs. (1) as

$$\vec{\phi}_t = \mathcal{L}_x\vec{\phi} + \mathcal{N}\vec{\phi}, \tag{19a}$$

where $\vec{\phi} = [\psi,\ \chi]^T$, $\mathcal{L}_x\vec{\phi}$ represents the linear x-derivative terms, and $\mathcal{N}\vec{\phi}$ represents all the terms on the right-hand side of (1), then one time step of the 2nd-order SSM is

$$\vec{\phi}^{\,n+1} = e^{\mathcal{O}_1\Delta t/2} e^{\mathcal{O}_2\Delta t} e^{\mathcal{O}_1\Delta t/2}\,\vec{\phi}^{\,n}. \tag{19b}$$

Here $\mathcal{O}_{1,2}$ stand for the pair $\mathcal{L}_x, \mathcal{N}$ taken in either order. Note that when two (or more) time steps are combined, the action of two consecutive $\exp[\mathcal{O}_1\Delta t/2]$'s can be implemented as one $\exp[\mathcal{O}_1\Delta t]$. Importantly, all substeps[2] involving $\mathcal{L}_x\vec{\phi}$ will require only the operation $\exp[\mathcal{L}_x(1\cdot\Delta t)]$, and therefore one can take $\Delta t = \Delta x$ to facilitate the MoC-based implementation (18) of this substep. (The presence of the first and last $\exp[\mathcal{O}_1\Delta t/2]$ does not present a problem since one can either choose $\mathcal{O}_1 = \mathcal{N}$ or implement *only those two* half-substeps by DFT or by interpolation of the grid.) In contrast, for 4th- and higher-order forms of the SSM, one would require substeps of the form $\exp[\mathcal{L}_x(\mathrm{const}\cdot\Delta t)]$ with $\mathrm{const} \neq 1,\ 1/2$. This either is incompatible with the MoC-based implementation (18), unless at *every* time step one uses an interpolation (whose effect on the stability of high-wavenumber harmonics is unknown), or may lead to a numerical instability of those high-wavenumber harmonics, as we will hypothesize in Appendix A.

We repeated the simulations for the parameters shown in Fig. 4, but using the MoC-SSM implemented as described above, with the $\mathcal{L}_x$-substep using the nonreflecting BC (12). We also used the absorber (14a), (15) at every time step. The level of the radiation was found to be below 10^{-6} and was essentially unchanged from $t = 1{,}000$ to $t = 10{,}000$, as previously for the MoC-ME. In fact, the solution looks very similar to that obtained by the MoC-ME (see Fig. 4(a)) and hence is not shown. Evolutions of this numerical solution's charge and Hamiltonian, as well as the deviation of the charge density's L_2-norm, are shown in Fig. 4(d). Note that these quantities show no trace of a systematic deviation, unlike what one observes in Fig. 4(b) for the MoC-ME.

3. Conclusions

We have resolved the recent controversy between the semi-analytical prediction [1] of linear stability of soliton (2) of the Gross–Neveu model (1) and the numerical observations of instability of that soliton with small values of the frequency [11,15]. We numerically demonstrated that the soliton is linearly stable up to the frequency values of $\Omega = 0.01$, which is an order of magnitude below the previously studied value of $\Omega = 0.1$, where earlier studies reported an instability. Using either of the numerical methods that we proposed, the MoC-ME or MoC-SSM with nonreflecting BC (12) and an absorber like (14a), it is possible to simulate solitons with yet smaller values of Ω and over longer times than the $t = 10{,}000$ reported above. We did not find it necessary, however, as the reported simulations showed no change in either the soliton nor dispersive radiation over such long times.

The key ingredient that allowed us to carry out these accurate and long-term simulations was the uncovering of the main "culprit" that caused the numerical instability of the soliton in some of the previous numerical studies. Once this culprit — the interaction of the soliton with its own dispersive radiation emitted due to discretization error — had been identified, it became clear how to suppress it (by a combination of nonreflecting and absorbing boundaries). We believe that the numerical methods used in this work can be employed to study long-term stability of solitons of Dirac equations with higher-order nonlinearities or with a different type of nonlinear field self-interaction [11], with an external potential [14], or of coupled Dirac equations [33].

[2] Except possibly the first and last ones.

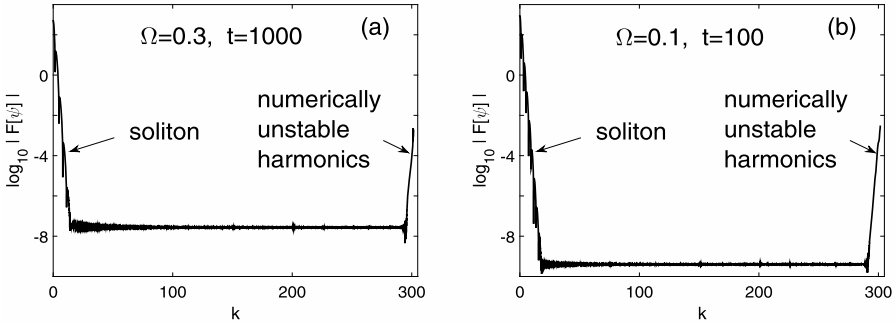

Fig. 5. Spectra of the numerical solution of Eqs. (1) obtained with the Fourier SSM. Values of Ω and simulation times are shown in the plots. Simulation parameters are: $L = 128$, $M = 3 \cdot 2^{12}$, $\Delta x \approx 0.01$, $\Delta t = 0.5\Delta x$. An initial value of 10^{-10} was added to each harmonic so that the numerical error would grow from that, controlled, level rather than from the machine round-off error.

Thus, on one hand, we have confirmed the theoretical prediction of the linear stability, as defined in the Introduction, of the Gross–Neveu soliton (2). On the other hand, we have also observed the previously reported increase of susceptibility of the soliton to small but finite perturbations, such a dispersive radiation, as Ω decreases. Finding a mechanism behind this increased susceptibility remains an open problem.

Acknowledgement

This work was supported in part by the National Science Foundation grant DMS-1217006. The author thanks the anonymous reviewers, whose constructive criticism helped to improve this paper.

Appendix A. Possible reason for numerical instability observed in [11]

Here we present a hypothesis as to why the 4th-order accurate MoC-SSM used in [11] exhibited a growth of highly oscillatory harmonics (i.e., a high-frequency numerical instability), as is evident from the captions to Figs. 5 and 6 in that paper. There are two ingredients to our hypothesis. First, we will show in a separate publication [34] that the SSM (with any BC) applied to Dirac equations may, under certain conditions (stated below), have numerically unstable modes near wavenumbers $k_{j\pi} = j\pi/\Delta t$, $|j| = 1, 2, \ldots$. In [11], one had $\Delta t = 12\Delta x$, where the factor '12' had to be used to implement a substep $\exp[\mathcal{L}_x \Delta t/12]$, which was part of a 4th-order accurate scheme, by the MoC. Thus, there were 12 potentially "dangerous" wavenumbers, $|k_{j\pi}| \le k_{\max} = \pi/\Delta x$, near which numerical instability could occur in [11].

Second, as we will also show elsewhere [34], the numerical instability near $k_{j\pi}$ of the *1st- and 2nd-order* SSM can occur only if the soliton is physically (as opposed to numerically) unstable. However, for a higher-order SSM (such as the 4th-order one used in [11]), there is expected to be *no* relation between the physical stability of the initial soliton and the numerical stability of harmonics with $k \approx k_{j\pi}$. We have not performed a detailed analysis for higher-order versions of the SSM for the Dirac equations, but it is known from such an analysis for the nonlinear Schrödinger equation [35] that the growth rate of numerical instability for higher-order SSM schemes is, in general, different from that for the 1st- and 2nd-order schemes. Therefore, even if there could be no high-frequency numerical instability of the 2nd-order SSM (19b), used in this work, there could be such an instability for higher-order SSM schemes. We think that this could be the reason behind the high-k numerical instability observed in [11]. However, a detailed investigation of this question is outside the scope of this work, whose focus is on demonstrating a long-term stability of Gross–Neveu solitons with small Ω.

Appendix B. Unconditional instability of the Fourier SSM for soliton (2) with small Ω

The purpose of this Appendix is to justify our *not* using the Fourier version of the SSM in this work.

The implementation of the Fourier SSM follows the outline for the MoC-SSM in Section 2.4, except that the operation $\exp[\mathcal{L}_x \Delta t]$ is performed by the DFT and its inverse; see [24,16,17] for more details. Let us recall that the use of DFT forces the BC to be periodic, and this is the only difference[3] between the Fourier SSM and the MoC-SSM which uses the nonreflecting BC (12).

This difference in BC, which may seem to be inconsequential for simulations of a soliton, which is zero to machine precision at the boundaries, leads to a dramatic difference in the behavior of high-wavenumber harmonics between the two versions of the SSM. In Fig. 5 we show the Fourier spectra of the numerical solution obtained with the Fourier SSM for two initial solitons, whose profiles are shown in Fig. 1. The soliton with $\Omega = 0.3$, which could easily be simulated by the MoC-ME even without the absorber (14a) (see the end of Section 2.2) up to $t = 10{,}000$, is destroyed before $t = 1{,}500$ when simulated by the Fourier SSM. The "culprit" is not only, and not primarily, the low-wavenumber radiation, discussed in Section 2.2, but the numerically unstable highest Fourier harmonics. This numerical instability becomes dramatically stronger as Ω decreases. For example, the growing highest Fourier harmonics destroy the soliton with $\Omega = 0.1$ (see Fig. 5(b)) already before $t = 200$. This should be contrasted with the performance of the MoC-ME, which can simulate this soliton up to $t = 1{,}000$ with the error below 10^{-6}: see Fig. 3.

Most unexpectedly, the observed numerical instability is *unconditional* [34]. That is, it persists for arbitrarily small Δt. For example, we obtained essentially the same results as those shown in Fig. 5 when we used $\Delta t = 0.001\Delta x$. This fact contradicts earlier statements about the stability of the Fourier SSM [24,17]. (Specifically, in [24] the stability threshold was said to satisfy $\Delta t_{\text{thresh}} = O(\sqrt{\Delta x})$, while in [17] the method was claimed to be unconditionally stable.)

References

[1] G. Berkolaiko, A. Comech, On spectral stability of solitary waves of nonlinear Dirac equation in 1D, Math. Model. Nat. Phenom. 7 (2012) 13–31.
[2] D.J. Gross, A. Neveu, Dynamical symmetry breaking in asymptotically free field theories, Phys. Rev. D 10 (1974) 3235–3253.

[3] Strictly speaking, the solution of the $\mathcal{L}_x$-substep obtained by the DFT is not exact, unlike that obtained by the MoC-based Eqs. (18). However, the approximation error introduced by the DFT is exponentially small, $\exp[-O(1/\Delta x)]$, and for practically relevant values of Δx the DFT solution of the $\mathcal{L}_x$-substep can be considered as exact.

[3] M. Soler, Classical, stable, nonlinear spinor field with positive rest energy, Phys. Rev. D 1 (1970) 2766–2769.
[4] S.Y. Lee, T.K. Kuo, A. Gavrielides, Exact localized solutions of two-dimensional field theories of massive fermions with Fermi interactions, Phys. Rev. D 12 (1975) 2249–2253.
[5] A. Alvarez, B. Carreras, Interaction dynamics for the solitary waves of a nonlinear Dirac model, Phys. Lett. A 86 (1981) 327–332.
[6] F. de la Hoz, F. Vadillo, An integrating factor for nonlinear Dirac equations, Comput. Phys. Commun. 181 (2010) 1195–1203.
[7] N. Boussaïd, S. Cuccagna, On stability of standing waves of nonlinear Dirac equations, Commun. Partial Differ. Equ. 37 (2012) 1001–1056.
[8] D. Pelinovsky, Y. Shimabukuro, Transverse instability of line solitary waves in massive Dirac equations, J. Nonlinear Sci. 26 (2016) 365–403.
[9] I.V. Barashenkov, E.V. Zemlyanaya, Oscillatory instability of gap solitons: a numerical study, Comput. Phys. Commun. 126 (2000) 22–27.
[10] N. Boussaïd, A. Comech, Spectral stability of small amplitude solitary waves of the Dirac equation with the Soler-type nonlinearity, arXiv:1705.05481.
[11] S. Shao, N.R. Quintero, F.G. Mertens, F. Cooper, A. Khare, A. Saxena, Stability of solitary waves in the nonlinear Dirac equation with arbitrary nonlinearity, Phys. Rev. E 90 (2014) 032915.
[12] A. Alvarez, M. Soler, Energetic stability criterion for a nonlinear spinorial model, Phys. Rev. Lett. 50 (1983) 1230–1233.
[13] I.L. Bogolubsky, On spinor soliton stability, Phys. Lett. A 73 (1979) 87–90.
[14] F. Mertens, N.R. Quintero, F. Cooper, A. Khare, A. Saxena, Nonlinear Dirac equation solitary waves in external fields, Phys. Rev. E 86 (2012) 046602.
[15] J. Cuevas-Maraver, P.G. Kevrekidis, A. Saxena, F. Cooper, F.G. Mertens, Solitary waves in the nonlinear Dirac equation at the continuum limit: stability and dynamics, in: Ord. Part. Diff. Eqs., Nova Science, Boca Raton, 2015, Chap. 4.
[16] J. Xu, S. Shao, H. Tang, Numerical methods for nonlinear Dirac equation, J. Comput. Phys. 245 (2013) 131–149.
[17] W.Z. Bao, Y.Y. Cai, X.W. Jia, J. Yin, Error estimates of numerical methods for the nonlinear Dirac equation in the nonrelativistic limit regime, Sci. China Math. 59 (2016) 1461–1494.
[18] X. Quan, H. Fu, S. Song, Structure-preserving wavelet algorithms for the nonlinear Dirac model, Adv. Appl. Math. Mech. 9 (2017) 964–989.
[19] R. Hammer, W. Pötz, A. Arnold, A dispersion and norm preserving finite difference scheme with transparent boundary conditions for the Dirac equation in (1+1)D, J. Comput. Phys. 256 (2014) 728–747.
[20] T. Colonius, Numerically nonreflecting boundary and interface conditions for compressible flow and aeroacoustic computations, AIAA J. 35 (1997) 1126–1133.
[21] W. Briggs, A.C. Newell, T. Sarie, Focusing: a mechanism for instability of nonlinear finite difference equations, J. Comput. Phys. 51 (1983) 83–106.
[22] D.M. Sloan, A.R. Mitchell, On nonlinear instabilities in leap-frog finite difference schemes, J. Comput. Phys. 67 (1986) 372–395.
[23] T.I. Lakoba, Long-time simulations of nonlinear Schrödinger-type equations using step size exceeding threshold of numerical instability, J. Sci. Comput. 72 (2016) 14–48.
[24] J. de Frutos, J.M. Sanz-Serna, Split-step spectral schemes for nonlinear Dirac systems, J. Comput. Phys. 83 (1989) 407–423.
[25] S. Shao, H. Tang, Interaction for the solitary waves of a nonlinear Dirac model, Phys. Lett. A 345 (2005) 119–128.
[26] T.I. Lakoba, Z. Deng, Stability analysis of the numerical method of characteristics applied to a class of energy-preserving hyperbolic systems. Part II: nonreflecting boundary conditions, http://arxiv.org/abs/1610.09080.
[27] D.F. Griffiths, D.J. Higham, Numerical Methods for Ordinary Differential Equations, Springer-Verlag, London, 2010, Chaps. 13 and 15.
[28] X. Antoine, W. Bao, C. Besse, Computational methods for the dynamics of the nonlinear Schrödinger/Gross–Pitaevskii equations, Comput. Phys. Commun. 184 (2013) 2621–2633.
[29] D. Givoli, B. Neta, High-order non-reflecting boundary scheme for time-dependent waves, J. Comput. Phys. 186 (2003) 24–46.
[30] D. Givoli, High-order local non-reflecting boundary conditions: a review, Wave Motion 39 (2004) 319–326.
[31] H. Yoshida, Construction of higher order symplectic integrators, Phys. Lett. A 150 (1990) 262–268.
[32] G. Strang, On the construction and comparison of difference schemes, SIAM J. Numer. Anal. 5 (1968) 506–517.
[33] A. Khare, F. Cooper, A. Saxena, Approximate analytic solutions to coupled nonlinear Dirac equations, Phys. Lett. A 381 (2017) 1081–1086.
[34] T.I. Lakoba, Study of (in)stability of the Fourier split-step method for the massive Gross–Neveu model, in preparation.
[35] T.I. Lakoba, Instability analysis of the split-step Fourier method on the background of a soliton of the nonlinear Schrödinger equation, Numer. Methods Partial Differ. Equ. 28 (2012) 641–669.